Journal of Asian Concrete Federation

journal homepage: https://jacf.sfulib3.publicknowledgeproject.org/index.php/jacf

Effect of Interfacial Failure on Stress-Strain Behavior of 3D-Printed Mortar Laminates

Ren Uematsu [a], Tomoko Fukuyama [b*], Hiroharu Kamada [c]

[a] *Graduate School of Science and Engineering, Ritsumeikan University, Nojihigashi 1-1-1, Kusatsu city, Shiga, 525-8577, Japan*
[b] *College of Science and Engineering, Ritsumeikan University, Nojihigashi 1-1-1, Kusatsu city, Shiga, 525-8577, Japan*
[c] *Polyuse Inc., Hamamatsucho Daiya Bldg. 2F, Hamamatsucho 2-2-15, Minato-ku, Tokyo, 105-0013, Japan*

ABSTRACT

Failure mechanisms of 3D-printed laminates reinforced with fibers are investigated. In order to clarify the effects of layered anisotropy in mortar filaments, compressive tests are conducted using specimens with end constraint under various loading rates. The specimens are cored-drilled in three directions from a laminated body fabricated by 3D printed, as well as those cast in a formwork. By reducing end-constraints, tensile stress is induced at the layer interfaces, and thus the interfacial fracture process is observed by using the Digital Image Correlation (DIC) method. In the core-drilled specimens, it was observed that the stresses drop sharply before reaching the maximum stress, followed by a subsequent recovery in load-bearing capacity. DIC confirmed that cracking initiated at the interfaces. These results were different from the specimens cast in the formwork. It is found that the interfacial failure of laminated mortar depends on the adhesion strength between the filaments. Thus, two-stage failure process is elucidated as an initial brittle fracture along a weak layer interface, followed by a tenacious post-peak response.

Keywords: 3D Printed for Construction, Laminated Interface, Stress-Strain relationship, Digital Image Correlation Method, Compressive Strength Test

1. Introduction

Development of 3D printing technology for construction has extensively advanced [1]. Currently a mainstream for printing technology is the extrusion method, which stacks filaments by extruding cement-based materials from a nozzle. However, it has been widely pointed out that the laminated interfaces (hereafter, interfaces) can lead to a reduction in structural and durability performance [2], giving rise to significant anisotropy [3].

While compressive loading from multiple directions using cubic specimens has been a common method for evaluating interfacial anisotropy, studies such as Wolfs et al. [4] evaluated the effects of printing parameters on interlayer adhesion and anisotropy using cubic specimens, and similarly, Surehali et al. [5] reported the influence of laminated height on compressive failure modes. This approach often suffers from stress concentrations at the corners of the specimen and end constraints caused by friction with the loading plates. These factors make it difficult to accurately evaluate behaviors unique to laminated bodies, such as interfacial sliding and debonding.

In this regard, the authors previously reported preliminary findings on the variations in stress-strain relationships [6] and initial DIC-based observations [7] using cylindrical specimens cored from 3D-printed laminates. While the experimental data in this paper are consistent with those in the earlier report [7], the present study provides an in-depth elucidation of the physical mechanisms governing the two-stage failure process. The potential factors for these variations were considered to include the influence of microscopic structures on anisotropy, such as the shape and orientation of internal voids associated with material flow during printing [8] and the minute lack of bonding at the interfaces [9]. In addition, the effects of differences in the restraint conditions at the top and bottom ends of the specimens were also considered [10].

It is well known that, in concrete specimens, nucleation of

* Corresponding author: Tomoko Fukuyama (tmkfkym@fc.ritsumei.ac.jp)

DOI http://dx.doi.org/10.18702/acf.2026.12.2.55

Received: 02-Nov-2025; Revised: 16-Feb-2026; Accepted: 23-Feb-2026; Published online: 21-May-2026

ISSN 2465-7964, eISSN 2465-7972.

failure under compressive loading originates from microcracks initially present in the interfacial transition zone [11]. As a result, in the laminated bodies, the layer interfaces could serve as the starting points of failure.

However, it is difficult to induce tensile failure caused by the adhesion of the weakest interface in a splitting tensile test. In this regard, it is considered that around the center of a cylindrical specimen, the tensile failure is to be observed at the interface with the lowest bond strength by reducing the end constraint in a compression test. Furthermore, the application of DIC is advancing as a method for evaluating localized deformation and propagation behavior (e.g., Yao et al. [12]). Nonetheless, most existing compressive tests are conducted under friction and loading rate conditions prescribed standard specifications, where the resulting data may be susceptible to noise caused by dynamic effects and end constraints.

In the present study, compressive tests are conducted to investigate the effect of filament anisotropy in laminates by reducing the end constraint under two loading rates. Stress-strain measurements and the image observation by DIC are made at the point where a characteristic stress-strain relationship is observed.

2. Experiment Overview

2.1 Specimens

The material used was a cement-based premix powder consisting of ordinary Portland cement, silica sand with a diameter of less than 2 mm, and reinforcing fibers with a length of 10 mm. Mortar was prepared with a water-to-powder ratio of 0.16. For the preparation of the mortar, a continuous mixing pump connected to a 3D printer was used, with the water-to-powder ratio 0.16 serving as the target value.

A gantry-type 3D printer, "Polyuse Zero" manufactured by Polyuse inc., was utilized for the fabrication of the specimens. The 3D printer (3DP) has a maximum build volume of 2500 mm in width, 1900 mm in depth, and 1600 mm in height. The nozzle diameter was 15 mm, and moving speed was set to140 mm/sec. Under these specifications, the resulting mortar filaments were approximately 30 mm wide and 10 mm thick.

Table 1 shows the conditions of the specimens. These are core-drilled with 100 mm in diameter and 200 mm in height from 300 x 300 x 300 mm cubic laminated block fabricated with the 3D printer, as shown in Fig. 1. Focusing on the lamination anisotropy, cores were drilled from three directions, which are labelled as the X, Y, and Z directions. Additionally, using the same premix powder material, specimens were prepared by casting into formworks of the same dimensions (hereafter, M).

In this study, a single specimen was tested for each condition to focus on visualizing the unique failure processes of 3D-printed laminates and elucidating their detailed mechanical mechanisms. While the sample size per condition is limited in this specific series of DIC measurements, the characteristic stress-strain responses, including the temporary drop and subsequent recovery of load-bearing capacity, have been consistently observed across multiple specimens in our preliminary experiments. Ensuring highly accurate DIC measurements at the exact same material age necessitated strict synchronization, which inherently limited the number of tests that could be conducted simultaneously under these precise conditions.

2.2 Measurements

One typical loading-rate for the specimen of 100 mm diameter and 200 mm height is 4.7 kN/sec, according to JIS A 1108-2018 [13]. Further, to investigate deformations associated with crack propagation, two levels of loading rate are set as Series 1 at 0.785 kN/sec and Series 2 at 1.17 kN/sec. Additionally, to reduce end constraints, 0.5 mm-thick Teflon sheets are placed on the top and bottom ends of the specimens, and silicone grease is applied in-between.

As shown in Fig. 2, five strain gauges (gauge length: 30 mm) are attached to the specimen. Of the two vertical strain gauge, one is attached avoiding the interface in the longitudinal direction of the specimen. This is because the possibility of gauge detachment during loading is taken into account. The three lateral strain gauges are attached with regular intervals to investigate the characteristics of deformation due to the reduction of end constraint and the effect of the interface in the short-side direction.

The strain distribution on the specimen surface is visually measured by DIC. As shown in Fig. 3, the area of the specimen without strain gauges (indicated in red) is applied as the measurement surface. After coating with white-base spray, a random pattern of measurement points is painted with black spray. Similar to the previous report [14], two cameras are installed in front of the specimen, and images are captured every two seconds.

Table 1 Test Specimen Conditions

Test Specimens	Direction	Number of Specimens	Curing Conditions (at 52 days)
Core-drilled	X	Series 1: 1 Each Series 2: 1 Each	30 days: In air (Cast: 2024/08/26, Fujisawa; Shipped: 09/04 Chigasaki; No temp./humidity control) +22 days: 20℃, 87% RH
	Y		
	Z		
Formwork	—		

DIC is a method that calculate the displacement before and after deformation, and determines the values and the directions of the maximum principal strain (tensile) and minimum principal strain (compressive). By making a color map of the surface strain [15], the factors contributing to the characteristic stress-strain relationship is to be studied by DIC.

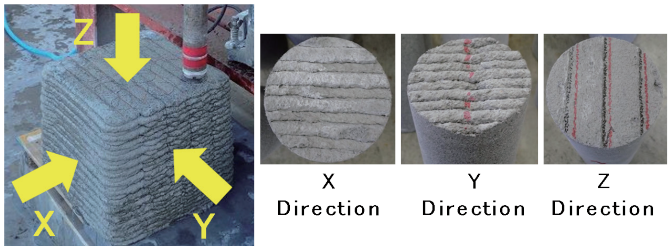

Fig. 1 Test Specimen Summary (Sampling Direction)

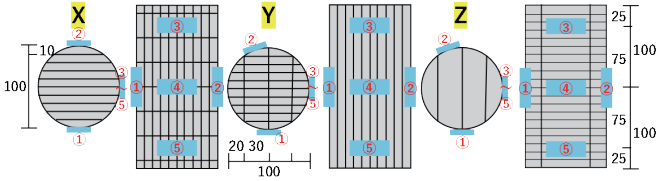

Fig. 2 Strain-gauge loctions of the specimen.

3. Experimental Results

3.1 Stress-Strain Relationship

Fig. 4 shows stress-lateral strain relations, while Fig. 5 shows stress-longitudinal strain relations for 3-directional core-drilled specimens in Series 1 and 2. Compared to those of formwork (M), strains at all gauge positions in the XYZ specimens vary widely with the progression of loading. In M specimens, less variations in lateral strains are observed that, as deformed more uniformly due to the reduction of end constraints. This implies that the variations in lateral strains of core-drilled specimens are to be caused by the presence of interfaces.

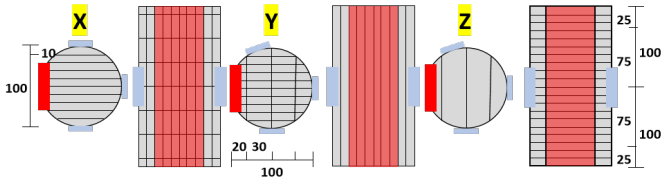

Fig. 3 DIC measurement locations of the specimenwhere

Further, the core-drilled specimens exhibited “S-shaped” stress-strain relations, or experienced final failure at lower stresses than M specimens. In the former relations, it is considered that failure occurred at the time of the first strain drop, and then subsequently the stress increased again until the ultimate failure was reached. Comparing the longitudinal strains of Series 1 and 2, the strain drops occurred later in Series 1 due to the slower loading rate, and the variations in longitudinal strain became larger.

Fig. 6 shows the stresses at the strain drop event (left column) and the stress at the ultimate failure event (right column) for all specimens. In X and Y specimens, the differences between the stresses at the strain drop and at the ultimate stress in Series 2 are larger, and the ultimate stresses are even higher than those of Series 1. In Z specimens, the differences between Series 1 and 2 are only observed in the stresses at each stage, suggesting as similar to those of the formwork specimens.

3.2 DIC Observations

In the following, results of Series 2, which exhibited more pronounced interlaminar failure characteristics, are discussed. Fig. 7 shows DIC images of all specimens, where the top row

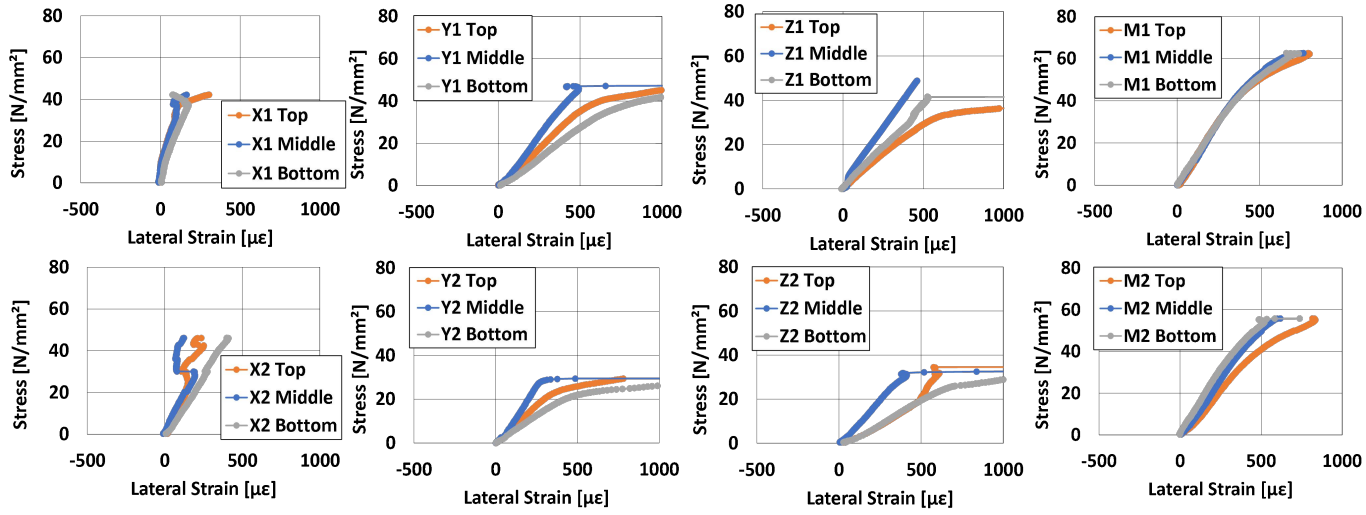

(a) X-direction sampled (b) Y-direction sampled (c) Z-direction sampled (d) M (Formwork)

Fig. 4 Stress-lateral Strain relations (Series 1 and 2, from top to bottom).

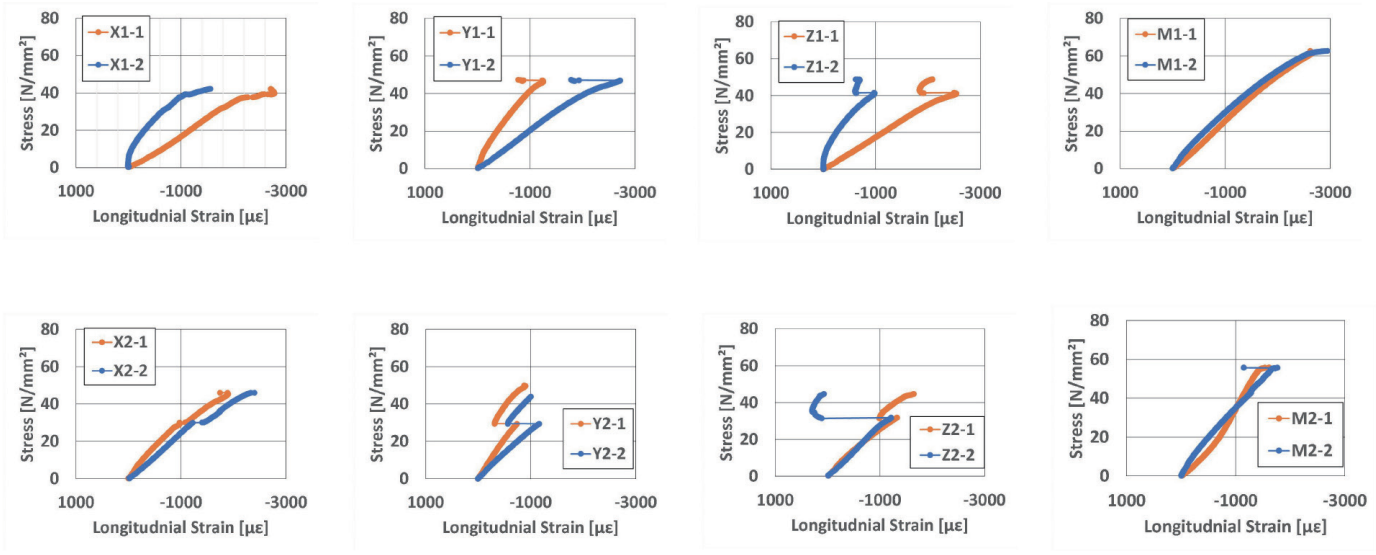

(a) X-direction sampled (b) Y-direction sampled (c) Z-direction sampled (d) M (Formwork)

Fig. 5 Stress-longitudinal strain Relations (Series 1 and 2, from top to bottom).

represents the maximum principal strain and the bottom row represents the minimum principal strain. Five images present stages at ① the start of the measurement, ③ the temporary strain drop, and ⑤ the ultimate failure, along with the intermediate images ② and ④ between them. Since specimen (d) does not have the temporary strain drop before the ultimate failure, the stages at equal intervals are shown. The color bars indicate that principal strain increases as the color approaches to red, while it decreases as it approaches to blue.

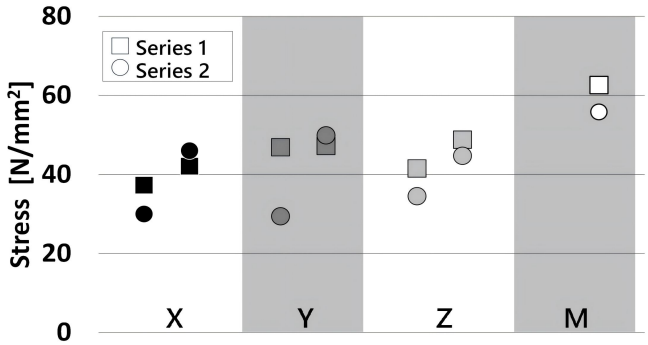

Fig. 6 Stress at strain drop and ultimate failure.

As shown in Fig. 7 (a), (b), and (c), it can be observed that longitudinal cracks occurred in the laminated specimens during the strain drop event (③). In particular, from the maximum principal strain in figures (a) and (b), symptoms of crack initiation (indicated in yellow) can be observed, suggesting that cracks propagated along the interfaces. In specimen (b) (Y-direction specimen), it is observed that cracks initiate from voids at the interfaces, as the laminated interfaces have been visually found even before the test. In contrast, specimen (c) shows a sudden crack initiation during the temporary strain drop. This is because no longitudinal interfaces are present at the surface. It is therefore considered that longitudinal cracks occur without symptoms, as similar to split tensile, as seen in specimen (d) (formwork M specimens). From the minimum principal strains in specimens (a) and (c), it can be seen that compressive strains occur in the lateral direction of the specimens. These phenomena are not observed in specimens (b) and (d), which have no visible interfaces. Thus, the compressive strains concentrate in the lateral directions.

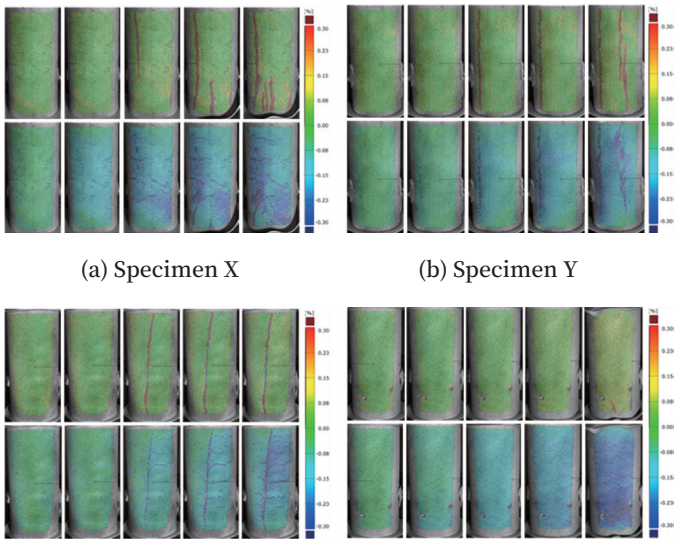

(a) Specimen X (b) Specimen Y

(c) Specimen Z (d) Specimen M

Fig. 7 DIC images of principal strains (Top: maximum principal strains, Bottom: minimum principal strains) from left to right, corresponding to specimens ① to ⑤ .

3.3 Failure Observation

Fig. 8 shows fractures of all specimens. In the leftmost

photograph, final failure conditions of the specimens are given. These were intentionally ruptured manually after the tests, to observe internal failure surfaces.

Cracks in the longitudinal directions of the specimens are observed at the surfaces other than those measured by DIC. Furthermore, as seen in the post-rupture photographs of specimens (a) and (b), clear split surfaces are observed at the cross-sections. This implies that cracks propagated along the interfaces. In contrast, cracks in specimen (c) propagate along the interfaces to some extent, but the upper part of the specimen is ruptured as another block as similar to that of specimens (d).

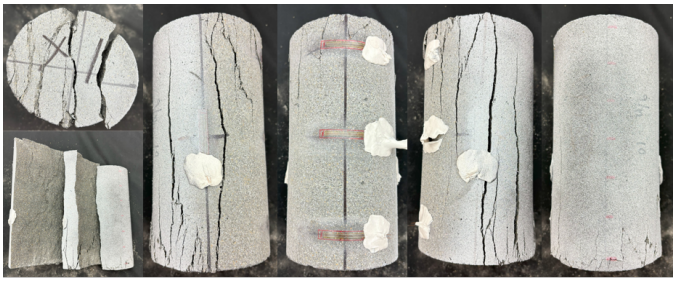

(a) Specimen X

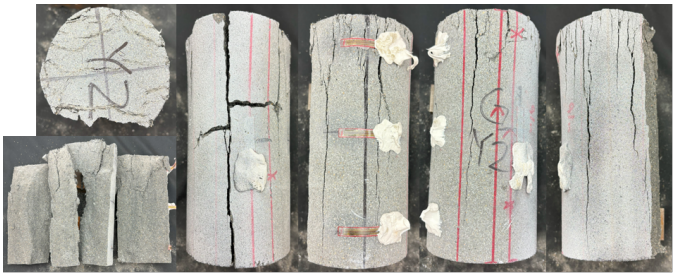

(b) Specimen Y

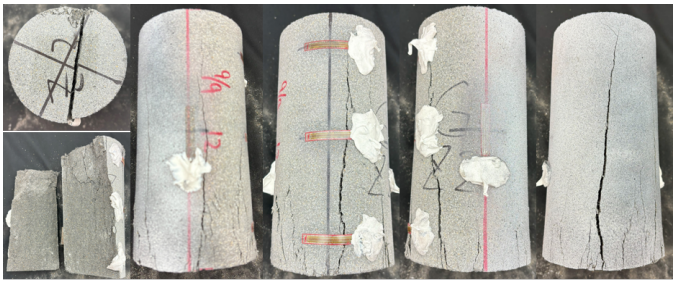

(c) Specimen Z

(d) Specimen M

Fig. 8 Fractures during compressive loading (Series 2).

4. Discussion on Failure Characteristics of Core-Drilled Specimens

4.1 Effect of End Constraints

The failure of M specimens indicates that crack propagation in the lateral direction is suppressed under compressive loading due to reduced end-constraint. It is known that final failure is similar to that of a split-tensile test, where vertical cracks are extensively nucleated. In the case of core-drilled specimens, this phenomenon could occur, depending on the bond strength between filaments as unique interface failure to laminated bodies. Thus, reducing the end-constraint and applying the tensile stress to the interfaces, 'two-stage failure process' is identified in the experiments.

4.2 Mechanism of the Two-Stage Failure Process

S-shaped stress-strain curves observed in the X- and Y-direction core-drilled specimens lead to a two-stage process, of an initial brittle failure as strain drop and a subsequent peak-stress recovery.

4.2.1 Stage 1: Brittle Interfacial Debonding

As confirmed by DIC observations, the dominant lateral tensile stress induced by the reduced end-constraint results in the debonding at the weak vertical interfaces. This leads to sudden brittle fracture even as strain drop. Furthermore, this interfacial debonding can be interpreted as the onset of a structural transition, in which the specimen transforms from a single integrated cylinder into multiple slender columnar elements separated by the interfaces.

4.2.2 Stage 2: Post-Peak Stress Recovery

During the 3D printing extrusion process, fibers tend to align parallel to the printing direction as parallel to the vertical interfaces. Therefore, in this study, we propose a mechanism involving following combined factors as the source of this tenacious behavior, enabling the columnar elements separated in Stage 1 to continue bearing compressive loads without premature buckling.

Aggregate Interlock:

The laminated interfaces possess surface roughness attributed to the stiffness of the extruded material [16]; thus, the fracture surfaces are not perfectly smooth but feature irregularities due to the aggregates. When the once-separated fracture surfaces come back into contact under compressive loading, these irregularities interlock, generating frictional resistance. This acts as a resisting mechanism against shear sliding between the elements, which is considered a contributing factor as to why the load-bearing capacity is not completely lost and a certain level of stress continues to be transferred.

Crack-Path Tortuosity and Interaction with Aligned Fibers:

The fracture does not propagate necessarily along the original interface plane. It could penetrate the filament body,

seeking the paths of least resistance tortuously. Then crack paths encounter the fibers that are aligned parallel to the interface. In order that the crack propagates further, either the fibers are to be pulled out from the matrix or are ruptured. This process absorbs energy and is thought to contribute to the overall stress recovery and to enhance toughness of the member.

The synergistic action of these two resisting mechanisms suppresses deformations, such as the independent buckling of the separated columnar elements. Consequently, it is inferred that stress redistribution occurred throughout the entire specimen, accompanied by high toughness, rather than terminating in a simple brittle failure. The factor which causes different two-stage failure processes by core-drilled direction is considered to be associated with lamination anisotropy. This is because the type and orientation of the weak planes that act as nucleation for final failure are closely related with the failure behavior of the specimens.

4.3 Effect of Laminate Anisotropy

The two-stage failure processes are observed in all cored specimens. However, their failure modes are different distinctly, depending on core-drilled directions. The fact could be associated with laminate anisotropy, resulting specifically from the type of "weak plane" that acts as the origin of rupture and the subsequent crack propagation. Thus, the anisotropy is investigated on the core-drilled directions.

Specimens cored-drilled in X- and Y-directions:

In these specimens, the lateral tensile stress acts as perpendicular to the vertical inter-layer interfaces, which become typical weak planes running through the entire specimen. As a result, failure propagates primarily along these interfaces, leading to dominant interfacial debonding, as evidenced by the separation at the cross-sections shown in Fig. 8 (a) and (b).

Specimens cored-drilled in Z-direction:

On the specimen cored-drilled in Z-direction, the initial strain drop suggests that the failure may also begin with an intra-layer interface failure between adjacent filaments, acting as nucleation point for final failure under lateral tensile stress. However, once a crack is nucleated, the subsequent failure propagation occurs as different from those of the X- and Y-directions. It is considered that the failure could become a composite mode involving "split-tensile failure" that propagates through the center of the specimen, rather than running through a specific interface. This would be a reason why the final failure state of the Z-direction specimen (Fig. 8 (c)) involves a few separations at the interfaces, in a similar manner to the failure characteristics of the M specimen (Fig. 8 (d)), and also ruptures integrated. From these observations, it is considered that the failure in the Z-direction specimen is of a composite mode as "split-tensile failure triggered at the interface."

The influence of horizontal interfaces on failure could result from another mechanism. Fig. 9 shows DIC images of the X and Z directions in the specimens, in which the interfaces exist horizontally. In the all specimens, distinct concentration of compressive strains is observed as linear patterns along the horizontal layer interfaces.

The layer interface is of mechanically weak due to lower stiffness than those of the filament. When the compression is applied to the entire specimen, this interfacial region undergoes larger compressive deformation (i.e., could be "crushed") than that of the surrounding filaments. The linear concentration of minimum principal strains observed by DIC can be interpreted as direct visualization of these localized compressive deformations at the interface. Furthermore, this localized compressive deformation goes beyond mere crushing. As the laminated interface is compressed longitudinally, it tends to expand laterally due to the Poisson effect. However, the adjacent high-stiffness filaments located above and below constrain this lateral expansion. Consequently, the deformation constraint caused by this stiffness differential generates localized lateral tensile stresses within the horizontal interface. While the end-restraint between the specimen and the loading plates was minimized in this study, these results suggest that internal constraints arising from the structural heterogeneity still govern the local failure process. In other words, the liner concentration of compressive strains represents not merely a region of large deformation, but rather an area where micro-damage propagates and accumulates due to mechanical constraints. Because this phenomenon is not observed in the Y-direction and M specimens without the horizontal interfaces, the finding is validly supported.

Thus, it is evident that the failure behavior of the laminated body is strongly governed by the orientation of the interfaces. In particular, longitudinal interfaces act as nucleation points of debonding failure due to lateral tensile stress, while lateral interfaces act as the nuclei of localized compressive deformation under compression. The effect of laminate anisotropy is, consequently, to be the fundamental reason for the failure modes, depending on the core-drilled orientations.

Up to this point, we have seen how the spatial factor of the layer interface orientation fundamentally determines the failure mechanism. Now, finally, let's consider how the temporal factor of 'loading rate,' another parameter in our study, influenced the manifestation of this failure.

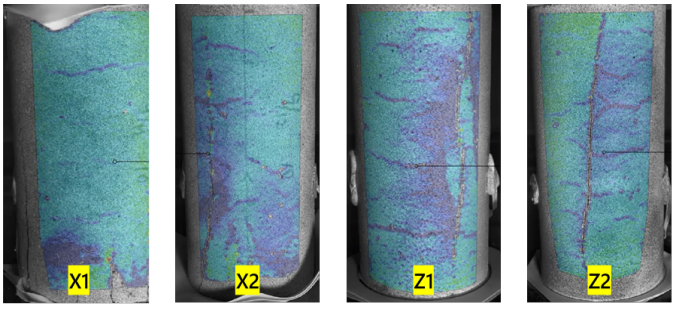

Fig. 9 DIC results of the specimen's interfaces in the lateral direction.

4.4 Effect of Loading Rates

The most significant effect of the loading rate in this study is clearly demonstrated by the stress differences shown in Fig. 6. Specifically, in Series 2 (fast loading), the magnitude of strength recovery from the initial stress drop to the ultimate stress is substantially larger than that in Series 1 (slow loading). This fact suggests that the post-failure behavior of the laminated specimens is strongly dependent on the loading rate. This phenomenon can be attributed to the dynamic behavior of the post-peak resistance mechanisms (i.e., aggregate interlock and interaction with fibers) that are activated in Stage 2.

Under Fast Loading (Series 2):

When the loading rate is high, microscopic failure processes such as sliding at the crack surfaces and fiber pull-out occur more abruptly. Under such dynamic conditions, the frictional resistance at the fracture surfaces and the pull-out resistance of fibers tend to be greater than under quasi-static conditions. In other words, the material exhibits a higher resistance to rapid deformation. This is inferred to be the primary reason why the material in Series 2 was able to recover to a much higher stress level after the initial failure, resulting in a larger stress difference.

Under Slow Loading (Series 1):

Conversely, at a slower loading rate, there is sufficient time for more stable crack propagation. The processes of friction and fiber pull-out proceed quasi-statically, minimizing any dynamic resistance-enhancing effects. Furthermore, the gradual application of load may allow damage to accumulate more diffusely throughout the specimen, rather than being concentrated at the primary crack plane. This could lead to the specimen reaching its overall capacity before a pronounced strength recovery, like that seen in Series 2, could fully develop.

From these considerations, it is concluded that the faster loading rate effectively enhanced the post-peak energy absorption capacity and toughness of the laminated specimens, resulting in an increase in their ultimate strength.

5. Conclusions

In compression tests of core-drilled samples from a 3-D printed concrete block, DIC observations of laminated interfaces were conducted with reduced end-constraint and loading rate. Depending on the core-drilled directions, the stress-strain relationships were investigated. The results are concluded, as follows.

1) It is confirmed that specimens with interfaces oriented parallel to the loading axis exhibit distinct two-stage failure processes, comprising an initial brittle fracture along the layer interface and a tenacious load-recovery response.

2) A hypothesis on a combined mechanism is proposed in order to explain the post-peak behavior, which is associated with aggregate interlock at the rough fracture surface and the interaction between a meandering crack path and fibers aligned in the printing direction.

3) The loading rate was found to strongly influence the post-peak behavior. A higher loading rate resulted in a significantly greater load-recovery capacity after the initial brittle fracture, suggesting that the material's energy absorption and toughness are enhanced under more dynamic loading conditions.

4) The findings demonstrate that the failure of 3DCP layered elements is not necessarily of a singular brittle mode. Elucidating this anisotropic failure mechanism provides foundational knowledge for the future development of materials and construction methods.

As for future work, to further generalize the failure mechanisms proposed in this study, the following challenges need to be addressed.

1) Statistical validation with an expanded number of specimens to confirm the broad applicability of the identified mechanisms across various printing parameters.

2) The combined mechanism involving aggregate interlock and fiber orientation proposed as a consistent mechanical model derived from the observed interfacial failure and strain redistribution. To further quantify the individual contributions of fiber reinforcement and physical interlocking, comparative experiments using fiber-free mortar are identified as a key direction for subsequent studies.

3) Future investigations utilizing microscopic internal observations, such as X-ray computed tomography (X-ray CT), are expected to provide direct validation of the internal cracking behavior and fiber-bridging effects proposed in this study.

CRediT authorship contribution statement:

-Ren Uematsu: Methodology, Carrying out the experiments, Writing - original draft

-Tomoko Fukuyama: Conceptualization, Supervision, Writing – review & editing

-Hiroharu Kamada: Methodology, Carrying out the experiments

Declaration of competing interest

The authors declare that they have no known competing financial interests or personal relationships that could have appeared to influence the work reported in this paper.

Acknowledgments

This research was conducted with the support of the Kajima Foundation, the Program for Optimizing Research Development, and the Japan Construction Information Center.

References

[1] Ogura, H., Abe, H., Kikuchi, R.; and Yamamoto, S. (2021). "Mechanical Property Evaluation of Fiber-Reinforced Cementitious Composites Fabricated by 3D Printing Layer-

by-Layer," Proceedings of the Japan Concrete Institute, 43(1), pp. 1379-1384 in Japanese
[2] Wolfs, R. J. M., Bos, F. P.; and Salet, T. A. M. (2018). "Early age mechanical behavior of 3D printed concrete: Numerical modeling and experimental testing," Cement and Concrete Research, 107, pp. 103-116
[3] Le, T. T., Austin, S. A., Lim, S., Buswell, R. A., Law, R., Gibb, A. G. F.; and Thorpe, T. (2012). "Hardened properties of high-performance printing concrete," Cement and Concrete Research, 42, pp. 558-566
[4] Wolfs, R. J. M., Bos, F. P.; and Salet, T. A. M. (2019). "Hardened properties of 3D printed concrete: The influence of process parameters on interlayer adhesion," Cement and Concrete Research, 119, pp. 132-140
[5] Surehali, S., Tripathi, A.; and Neithalath, N. (2023). "Anisotropy in Additively Manufactured Concrete Specimens under Compressive Loading—Quantification of the Effects of Layer Height and Fiber Reinforcement," Materials, 16(15), 5488
[6] Uematsu, R., Fukuyama, T.; and Kamada, H. (2024). "Experimental Study on Anisotropy and Performance Degradation in 3D-printed Construction Laminates," Summaries of Technical Papers of the Annual Meeting, Architectural Institute of Japan, pp. 1235-1236 in Japanese
[7] Kong, S., Uematsu, R., and Fukuyama T., (2025). "Experimental Study on the Influence of Laminated Interface Failure on the Compressive Loading Response of 3D Printed Mortar Laminates for Construction," Summaries of Technical Papers of the Annual Meeting, Architectural Institute of Japan, pp. 1529-1532 in Japanese
[8] Song, X., Xu, Q., Wang, H., Sun, X.; and Xue, F. (2025). "Flowability-Dependent Anisotropic Mechanical Properties of 3D Printing Concrete: Experimental and Theoretical Study," Applied Sciences, 15(11), 6070
[9] Li, F., Xiao, S., Yang, B., Li, K., Zhou, Y., Li, X.; and Liu, G. (2024). "Mechanical properties and anisotropy of 3D-printed concrete modified with multiscale materials based on optimized printing process design," Construction and Building Materials, 411, 134460
[10] Hayashi, N., Morimoto, Y.; and Hashimoto, C. (2018). "Effect of Loading Surface Flatness of Concrete Compressive Strength Test Specimens on Compressive Strength," Proceedings of the Japan Concrete Institute, 40(1), pp. 369-374 in Japanese
[11] Mehta, P. K.; and Monteiro, P. J. M. (Supervised translation by Tazawa, E., et al.). (1998). Concrete: Microstructure, Properties, and Materials, GIHODO SHUPPAN Co., Ltd., Tokyo, Japan. (In Japanese)
[12] Yao, Y., Zhang, J., Sun, Y., Pi, Y., Wang, J.; and Lu, C. (2024). "Mechanical properties and failure mechanism of 3D printing ultra-high performance concrete," Construction and Building Materials, 447, 138108
[13] Japanese Standards Association. (2018). "JIS A 1108:2018 – Method of test for compressive strength of concrete," Japanese Standards Association, Tokyo, Japan. (In Japanese)
[14] Shao, Y.; and Fukuyama, T. (2025). "Voltage Fluctuations due to Cracks in Cement Paste Caused by Cyclic Loading," AIJ Journal of Technology and Design, 77, pp. 30-35 in Japanese
[15] Demizu, A., Itai, S., Mifune, K.; and Matsuda H. (2011). "Fundamental Study on Strain Measurement of Construction Material by Digital Image Correlation Method," Reports of the Faculty of Engineering, Nagasaki University, 41(76), pp. 66-72 in Japanese
[16] Marchment, T., Sanjayan, J.; and Xia, M. (2019). "Method of enhancing interlayer bond strength in construction scale 3D printing with mortar by effective bond area amplification," Materials & Design, 169, 107684